

Evolution of environment dependent galaxy properties in the Sloan Digital Sky Survey

Ana Laura O’Mill,^{1*} Nelson Padilla,² Diego García Lambas,^{1,3}

¹*Grupo de Investigaciones en Astronomía Teórica y Experimental, IATE, Observatorio Astronómico, Universidad Nacional de Córdoba, Laprida 854, X5000BGR, Córdoba Argentina*

²*Departamento de Astronomía y Astrofísica, Pontificia Universidad Católica de Chile, V. Mackenna 4860, Santiago 22, Chile.*

³*Consejo de Investigaciones Científicas y Técnicas (CONICET), Avenida Rivadavia 1917, C1033AAJ, Buenos Aires, Argentina*

Released 2006 Xxxxx XX

ABSTRACT

We use photometric redshifts to analyse the effect of local environment on galaxy colours at redshifts $z \lesssim 0.63$ in the SDSS data release 6. We construct mock SDSS-DR6 catalogues using semi-analytic galaxies to study possible systematic effects on the characterisation of environment and colour statistics due to the uncertainty in the determination of redshifts. We use the projected galaxy density derived from the distance to the nearest neighbours with a suitable radial velocity threshold to take into account the uncertainties in the photometric redshift estimates. Our findings indicate that the use of photometric redshifts greatly improves estimates of projected local galaxy density when galaxy spectra are not available. We find a tight relationship between spectroscopic and photometric derived densities, both in the SDSS-DR6 data (up to $z = 0.3$) and mock catalogues (up to $z = 0.63$).

At $z = 0$, faint galaxies show a clear increase of the red galaxy fraction as the local density increases. Bright galaxies, on the other hand, show a constant red galaxy fraction. We are able to track the evolution of this fraction to $z = 0.55$ for galaxies brighter than $M_r = -21.5$ and find that the fraction of blue galaxies with respect to the total population progressively becomes higher as the redshift increases, at a rate of 15%/Gyr. Also, at any given redshift, bright galaxies show a larger red population, indicating that the star-formation activity shifts towards smaller objects as the redshift decreases.

Key words: cosmology: theory - galaxies: formation - galaxies: evolution - galaxies: Large scale distribution

1 INTRODUCTION

The study of galaxies in the field and in clusters has revealed the existence of significant correlations between several galaxy properties and their environment. In a pioneering work by Dressler (1980), it was shown for the first time that Galaxy morphologies depend on the local galaxy density. The decrease in the SFR of galaxies in dense environments is a universal phenomenon over a wide range of densities. For instance, Gómez et al. (2003) found that the star formation rate (SFR) of galaxies is strongly correlated with the local galaxy density; Balogh et al. (2004) characterise the environment using projected and three-dimensional densities concluding that the present-day correlation between star formation rate and environment is a result of short-timescale mechanisms that take place preferentially at high redshift, such as starbursts induced by galaxy-galaxy interactions (see also Baldry et al. 2004). However, these studies concern the nearby universe where spectroscopic redshifts allow for estimates of the local density of galaxies. At higher red-

shifts, spectroscopy is not available for large galaxy samples, and in consequence, the relation between galaxy properties and environment is more poorly understood. An alternative solution to this problem is the use of multi-band photometry to constrain galaxy redshifts. These techniques have been extensively studied (e.g., Koo 1985; Connolly et al. 1995; Gwyn & Hartwick 1996; Benítez 2000; Bolzonella et al. 2000; Csabai et al. 2003; Collister & Lahav 2004), and have proved to be efficient in estimating redshifts for large numbers of galaxies, which opens the possibility of obtaining their intrinsic properties for statistical studies.

One exception to this necessity is that of the VIMOS VLT Deep Survey, for which Cucciati et al. (2006) make use of the available spectroscopic redshifts to estimate local densities; however, their sample is small containing only 6582 galaxies out to $z = 1.5$. Their results show that massive galaxies shift towards redder values for lower redshifts, where only faint galaxies show a blue galaxy population. On the other hand, the use of photometric redshifts to study the evolution of galaxy colours at redshifts higher than $z = 0.3$, has only been attempted a few times, in part due to the difficulty in ensuring an accurate statistical measurement of

* E-mail: aomill@oac.uncor.edu

local density. For instance, Ienna & Pelló (2006) study the colour distribution of galaxies in the CFHTLS-Deep Field Survey¹ for redshifts in the range $0 < z < 1.3$, using a well calibrated photometric redshift estimator, New-HyperZ², to find results consistent with those from the VIMOS VLT Deep Survey, indicating the validity of the photometric redshift approach. De Lucia et al. (2007), find that the population of cluster galaxies in the Las Campanas Distant Cluster Survey (Gonzalez et al., 2001) shows a clear deficit of blue galaxies in low redshift galaxies with respect to clusters at $z \sim 0.8$. The variation of galaxy colours as a function of redshift provides important information on the stellar formation history of galaxies; De Lucia et al. fit their results with models where the star formation is suppressed early on in hostile cluster environments.

In this paper we analyse galaxy properties and their relation to the environment by means of photometric data taken from the Sloan Digital Sky Survey, Data Release 6 (SDSS-DR6, York et al. 2000). We use galaxy photometric redshifts, z_{phot} , from the SDSS database, to compute local densities, intrinsic luminosities and colours. The main advantage of our study is the comparatively large number of galaxies in the SDSS-DR6, at redshifts $0.1 < z < 0.63$, a range where deep spectroscopic surveys only offer a limited number of objects, and wide spectroscopic surveys are badly affected by selection biases.

This paper is organised as follows. In Section 2 we describe the data used in our analysis, both observational and from models of galaxy formation, Section 3 discusses the photometric redshifts available in the SDSS-DR6 and analyses their advantages and limitations. Section 4 describes the method used to calculate projected galaxy densities, Section 5 studies the evolution of galaxy colours as a function of their environment with redshift, and finally, Section 6 summarises the results obtained in this work.

Throughout this paper, we adopt the cosmological model characterised by the parameters $\Omega_m = 0.25$, $\Omega_\Lambda = 0.75$ and $H_0 = 70 \text{ h km s}^{-1} \text{ Mpc}^{-1}$.

2 THE GALAXY SAMPLES

The samples of galaxies used in this work are drawn from the catalogue of galaxies with photometric redshifts (z_{phot}) in the SDSS-DR6 (Oyaizu et al. 2008, available in the SkyServer). These photometric redshifts are obtained using the Artificial Neural Network (ANN) technique to calculate z_{phot} and the Nearest Neighbor Error (NNE) method to estimate z_{phot} errors for ~ 77 million, $r < 22$ objects classified as galaxies in the SDSS-DR6. In the remainder of this paper, we restrict all our analysis to samples with $r < 21.5$ since this magnitude limit ensures a good photometric quality and a reliable star-galaxy separation (Stoughton et al., 2002, Scranton et al., 2002). We use the spectroscopic Main Galaxy Sample (MGS; Strauss et al. 2002) to test the reliability of photometric redshift estimates, and their ability in predicting projected local galaxy densities. The MGS comprises all galaxies in the SDSS-DR6 brighter than a Petrosian magnitude $r_{\text{lim}} = 17.77$, with a median redshift $z \sim 0.1$.

The SDSS-DR6 provides imaging data in five bands, *ugriz*, and spectroscopy over $\simeq \pi$ steradians in the northern Galactic cap, and 225 square degrees in the south Galactic cap. The five broad bands *u*, *g*, *r*, *i*, and *z* (Fukugita et al. 1996; Hogg et al. 2001;

Smith et al. 2002), have effective wavelengths of 355, 467, 616, 747, and 892 nm respectively. For details regarding the SDSS camera see Gunn et al. (1998), for astrometric calibrations, see Pier et al. (2003). SDSS-DR6 imaging data covers a contiguous region of the north Galactic cap. In this paper we use de-reddened model magnitudes K-corrected using V4.1 of the publicly available code described in Blanton & Roweis (2006). We also repeat all the analysis presented in this work using alternative K-correction algorithms based on a grid of Bruzual & Charlot (2003) models, and find that our results do not change in a significant way.

We will study the dependence of galaxy colour on environment for subsamples of different galaxy luminosities (samples L1 to L4, see Table 1) and redshifts. Given that galaxies at increasingly large distances subtend an ever smaller angle on the sky, it is expected that the size of the PSF of the image (due to seeing) will eventually become larger than the apparent galaxy size. Such an effect would bias our sample against compact objects at large distances, in turn affecting our statistical measurements of the evolution of intrinsic galaxy properties. Therefore, we need to define our luminosity samples by taking into account both, the distance out to which we have a volume limited sample, and also the distance out to which the samples are free from selection effects due to the PSF. The former is done by direct measurement on the Hubble diagram (absolute magnitude vs. redshift), while in order to obtain the latter we proceed as follows. We use a low redshift sample composed by all galaxies in the range $0.04 < z < 0.08$. We divide this sample according to the luminosity limits that define our subsamples. We measure r_{10} , the 10 percentile of the distribution of physical galaxy radio, and calculate the maximum redshift out to which r_{10} subtends more than 1.5 arcsec. We take this limit as the typical seeing affecting the SDSS photometry (see for instance, Stoughton et al., 2002). This defines the maximum redshift (z_{max}) that ensures that compact galaxies in our samples are not confused with the PSF of the image. Table 1 also contains r_{10} as well as this maximum redshift for each of our luminosity subsamples. We will restrict the analysis to this maximum redshift from this point on; the table also shows the maximum redshift out to which the MGS (spectroscopic survey) can be used to construct volume limited samples, and as can be seen, z_{max} , the furthest we can reliably use the photometric catalogue, allows us a one order of magnitude increase in sample size with respect to the MGS.

2.1 Mock SDSS-DR6 catalogues

We construct mock SDSS catalogues using the semi-analytic model (SAM) from Bower et al. (2006), which is applied to the Millennium Simulation (Springel et al., 2005) outputs, to follow different processes that shape the galaxy population as time progresses, corresponding to a Λ CDM cosmology. The Millennium simulation consists of 2160^3 particles in a box of $500h^{-1} \text{ Mpc}$ a side, for a particle mass resolution of $8.6 \times 10^8 h^{-1} \text{ M}_\odot$. The resulting galaxies conform a complete sample down to a magnitude $M_r = -17$.

For each mock observer we apply the same angular mask affecting the photometric SDSS-DR6 sample, and apply a magnitude limit cut of $r_{\text{lim}} = 21.5$ (observer-frame apparent magnitudes). We store all the observed properties of galaxies, such as redshift (which includes the peculiar motion), angular position in the sky, and apparent magnitudes in several bands. However, the main advantage of the mock catalogue is that we also store several intrinsic properties such as the luminosity in different bands.

We produce two separate mock catalogues down to $r_{\text{lim}} = 21.5$. i) The first one uses the $z = 0$ SAM output as the source of

¹ http://www.ast.obs-mip.fr/users/rosier/CFHTLS_T0003

² <http://www.ast.obs-mip.fr/users/rosier/hyperz>

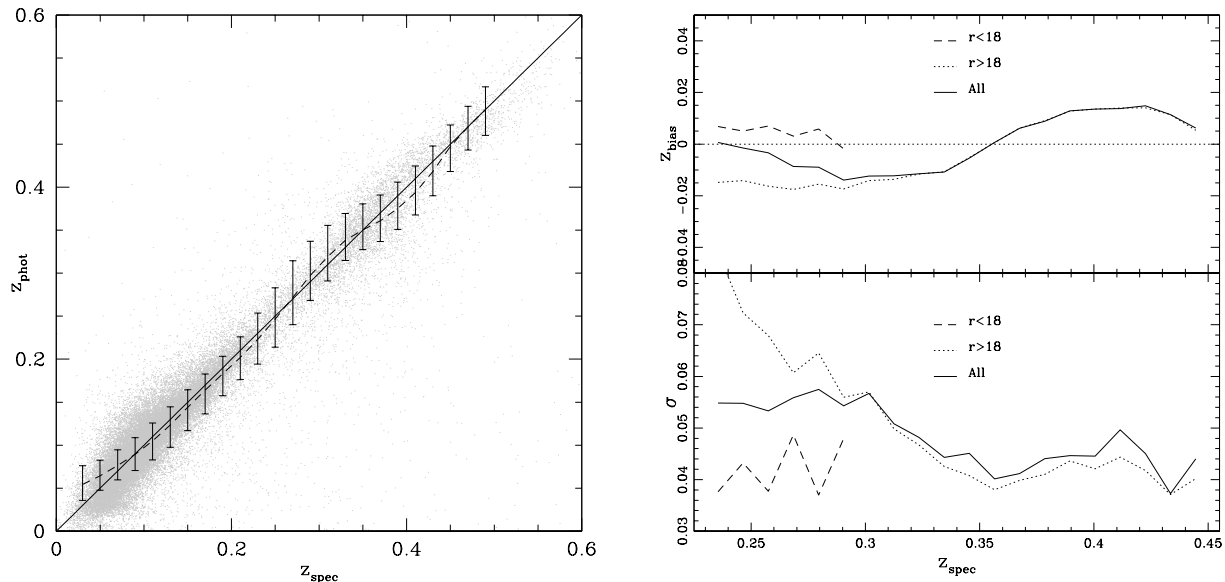


Figure 1. Left panel: z_{spec} vs z_{phot} relation for the SDSS-DR6 (dashed line); errorbars correspond to the 10 and 90 percentiles. Values corresponding to individual galaxies are shown as grey dots (shown for the 10% of the sample). The solid line shows the one-to-one relation. The error bars correspond to 2σ deviations. Right panels: systematic (top right) and stochastic (bottom right) errors in the photometric redshift estimates, for different apparent magnitude ranges (see the figure key).

Table 1. Definition of subsamples. The second and third columns show the maximum and minimum rest frame r-band absolute magnitudes of the sample, respectively. The fourth column shows r_{10} , the first 10% percentile of the galaxy size distribution at $z < 0.08$. The fifth, sixth and seventh columns are the redshift limits corresponding to volume-limited MGS, photometric $r < 21.5$ sample, and the maximum redshift out to which galaxies can be identified without risk of confusion with the PSF using r_{10} , respectively.

Sample	Minimum M_r	Maximum M_r	$r_{10}/h^{-1}\text{kpc}$	V. limited MGS z	V. limited photometric cat.	z_{max}
L1	-18.0	-16.0	1.8	0.02	0.10	0.08
L2	-19.5	-18.0	3.1	0.05	0.23	0.14
L3	-21.0	-19.5	4.7	0.09	0.41	0.23
L4	-21.5	-21.0	8.9	0.17	0.74	0.46
L5	-23.0	-21.5	11.7	0.21	0.91	0.63

model galaxies out to the highest redshift, which is simply defined by the selection function of the actual SDSS-DR6. ii) The second mock catalogue uses different outputs from the SAM to take into account the evolution of the galaxy population out to $z = 0.8$.

In both cases, photometric redshifts are assigned following a Monte-Carlo procedure that replicates the observed systematic and stochastic errors in the determination of photometric redshifts in the real SDSS-DR6. We acknowledge that this method only contains information from galaxies in the MGS, but since this includes a considerable number of galaxies at redshifts $z > 0.3$, we are able to assign photometric redshifts throughout the whole redshift range. We did not attempt to replicate the z_{phot} algorithm applied to the real SDSS-DR6 due to its complexity, and specially given the good observed behaviour of the error distribution of photometric redshifts in the real data, which we review in detail in the following section.

3 PHOTOMETRIC REDSHIFT ESTIMATES

Photometric redshift techniques use broadband photometry to perform an estimate of a galaxy redshift. This technique can be used to infer large numbers of galaxy distances efficiently including much fainter galaxies than spectroscopic measurements which require using large telescopes. There exist different techniques to estimate photometric redshifts which can be classified into two groups. The first set of techniques makes use of a small set of model galaxy spectra derived from empirical- or model-based spectral energy distributions. These methods reconstruct the observed galaxy colours by finding the best combination of template spectra at different redshifts (Benitez 1998; Bolzonella et al. 2000; Csabai et al. 2003). The fact that these methods rely on a small number of template SEDs, is their main disadvantage, in particular for populations at higher redshifts. On the other hand, there are techniques that need a large amount of prior redshift information (training set) called empirical methods (Connolly et al. 1995; Brunner et al. 1999). Their goal is to derive a parametrisation for the redshift as a function of the photometric parameters, inferred from the training set. The

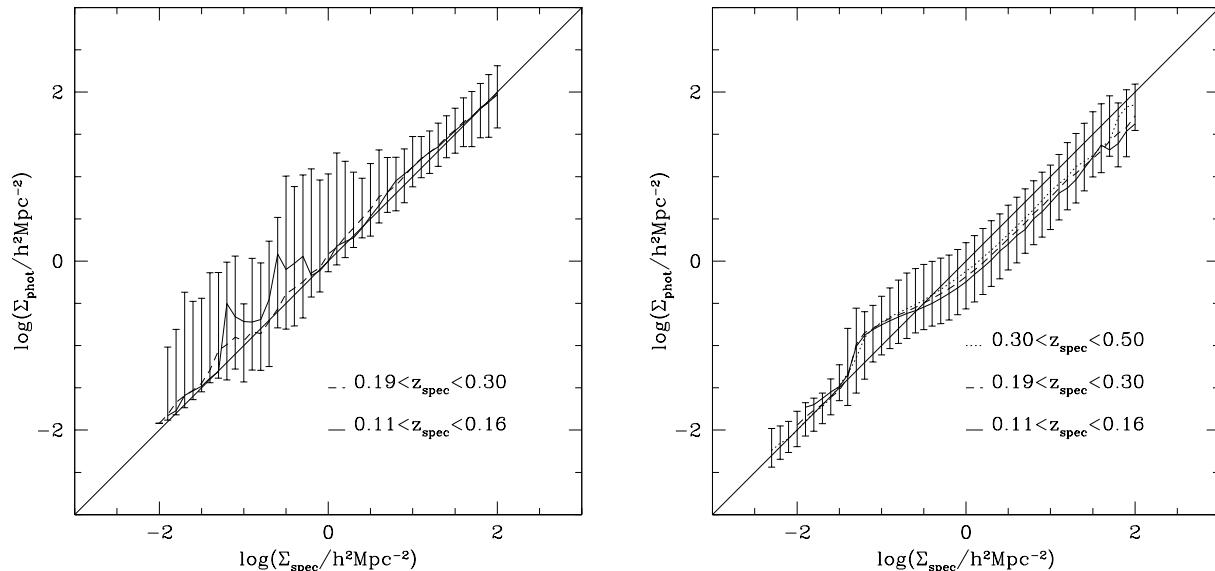


Figure 2. Correlation between spectroscopically (Σ_{spec}) and photometrically (Σ_{phot}) derived projected local galaxy densities, for different redshift ranges (shown in the key). SDSS-DR6 and mock results are shown in the left and right panels, respectively. The errorbars enclose 80% of the distribution with the mean shown by thick solid lines.

photometric parameters can be combinations of galaxy magnitudes in different photometric bands, galaxy colours, and concentration indexes.

In this work we use the Oyaizu et al. (2008) z_{phot} catalogue CC2, which uses colours and concentration indexes as their training set. The left panel of Fig. 1 shows the spectroscopic (z_{spec}) vs. z_{phot} redshift for a 10% of the objects in the SDSS-DR6 MGS. The figure shows the one-to-one relation as a solid line, and the median (dashed line), and 10 and 9 = percentiles (errorbars) of the scatter plot. Interesting points to notice are i) the lack of important concentrations of outliers, and ii) the small dispersion around the one-to-one relation, indicating very precise estimates of redshifts. This can be more clearly seen in the right panel of this figure, where we show the systematic differences between z_{phot} and z_{spec} , z_{bias} ; the lower sub-panel shows the variance, σ , we notice that $\sigma \sim 0.05$ at $z_{\text{spec}} > 0.3$.

4 CHARACTERISING GALAXY ENVIRONMENTS

We now address the accuracy of the use of photometric redshifts to characterise galaxy environments. In order to do this we use both photometric and spectroscopic redshifts in the SDSS-DR6 MGS to compute the projected galaxy densities using nearest neighbours in the plane of the sky. This is done in both, real and mock catalogues using an extension of the 5–th nearest neighbour local density estimator, Σ_5 . In our case, since our samples are not volume-limited, we need to account for a varying average galaxy density as a function of redshift. Therefore, we calculate the completeness of the survey at the redshift of a centre galaxy and use it to decide the most appropriate number of neighbours to calculate the density in such a way that these correspond to comparable volumes across the full range of redshifts. In our case, the number of nearest neighbours, brighter than $M_r - 5 \log(h_{70}) < -21$, is allowed to fluctuate

between 5 and 10; nearby galaxies will use larger numbers of neighbours than galaxies at higher redshifts, where the completeness is lower. The other important aspect of a projected density is that of selecting galaxies within a given range of radial velocity difference (ΔV). In the case of a spectroscopic survey, one needs to take into account the velocity dispersion inside virialised structures rather than the redshift measurement error (which is of the order of 100km/s); in photometric redshift surveys, on the other hand, the most important contribution to the smearing of structure in the direction of the line of sight is the z_{phot} error, which can be larger than the expected virialised motions. We have tested the correlation between Σ_5 for spectroscopic and photometric redshift data in SDSS-DR6 ($z < 0.3$) adopting a fixed $\Delta V = 1,000\text{km/s}$ for z_{spec} data and a varying ΔV in the range 1,000–3,000km/s for z_{phot} , taking into account the variation of the error in z_{phot} with galaxy magnitude (taken from Oyaizu et al. 2008). The results of this study show that the best correlation occurs for a value of ΔV corresponding to $\simeq 30\%$ of the error in the photometric redshift estimate. The maximum velocity difference allowed in our analysis is 4,000km/s. These improvements to the projected density estimator allow us to significantly improve the accuracy of the density estimates using photometry only data.

Figure 2 shows the relation between projected densities calculated using spectroscopic (x-axis, Σ_{spec}) and photometric (y-axis, Σ_{phot}) redshift estimates in the SDSS-DR6 (left) and the no-evolution mock (right) catalogues, for different redshift ranges (solid and dashed for low and higher redshifts, respectively; additionally, the mock catalogue results for even higher redshifts are shown in dotted lines). Errorbars enclose 80% of the distribution and is only shown for the high redshift densities (the dispersion in the relation does not show important changes with redshift), and the solid line shows the one-to-one relation. As it can be seen, the SDSS and mock catalogues show a very good agreement between spectroscopic and photometric projected densities, although there

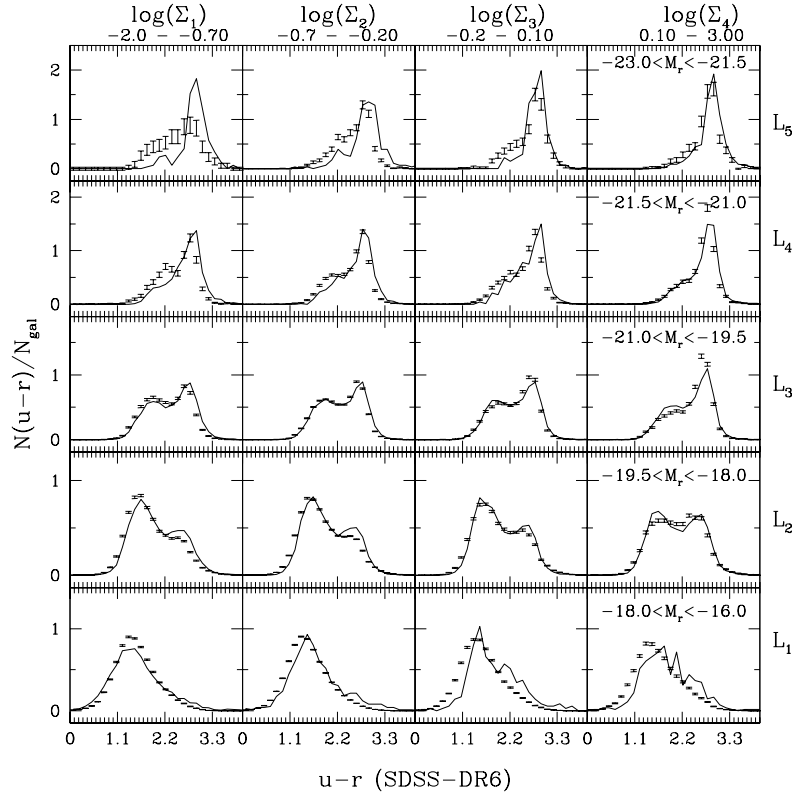


Figure 3. Distributions of $u-r$ colours in the SDSS-DR6 for different ranges of projected density (increasing from left to right in each panel; the units, not shown to improve clarity are $[\Sigma] = 1/h^2\text{Mpc}^{-2}$) and luminosities (increasing from bottom to top). Small errorbars show the results from photometric redshifts and are computed assuming Poissonian statistics. Solid lines show the results obtained using spectroscopic redshifts. We only show galaxies with $z < 0.08$.

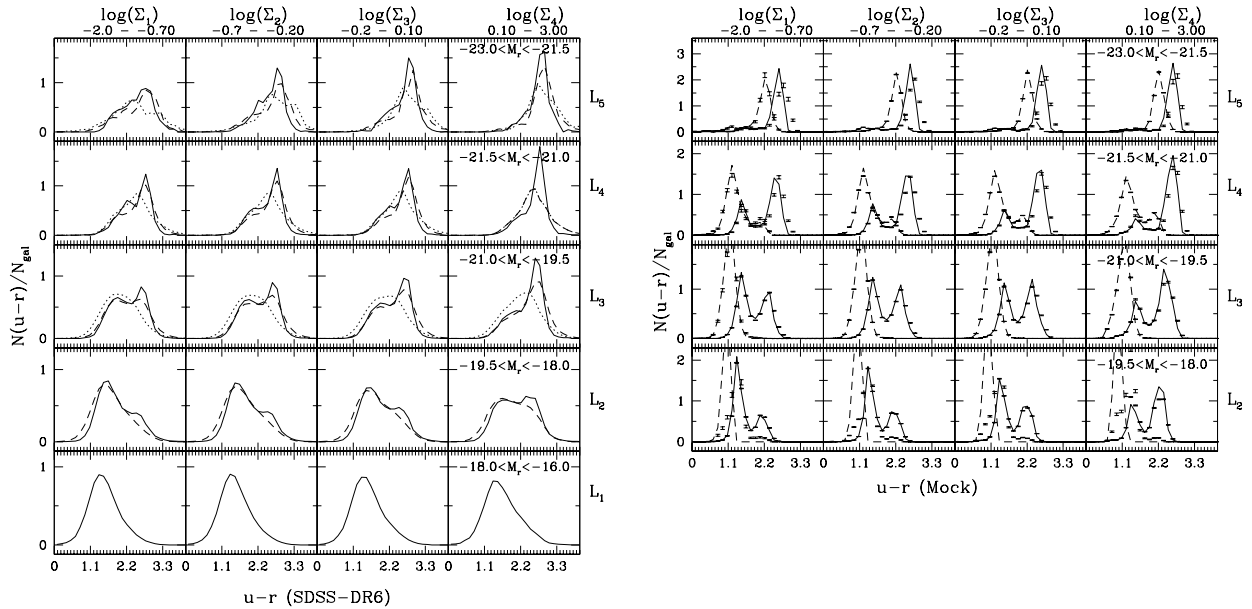


Figure 4. Colour distributions for SDSS-DR6, and evolving mock catalogues (left and right, respectively) as a function of luminosity (bottom to top, see the key in the right-most subpanels) and local density (left to right, units are as in Figure 3), for different median redshifts $z = 0.062, 0.124, 0.19$ (solid, dashed and dotted lines, respectively, left panel only) and $z = 0.08$ and 0.5 (solid and dashed lines, respectively, right panel only).

is a slight tendency for SDSS-DR6 photometrically derived densities to show a high density tail. Notice that the errors in the projected densities shown for the mock correspond to a much higher redshift than the SDSS-DR6; this is to check that the estimates of density are also accurate at redshifts higher than those accessible using the SDSS-DR6 MGS. Another effect that should be taken into account is the SDSS-DR6 minimum fiber separation ($55''$) which could affect the results from the spectroscopic data. We use the mock catalogue to study this effect on the deepest spectroscopic sample we use in this work, $z \sim 0.3$, and find that Σ_{spec} can be underestimated by only an average of a 1%.

5 EVOLUTION OF ENVIRONMENT DEPENDENT GALAXY PROPERTIES

We now explore the effects of environment on galaxy colours at different redshifts. We start by comparing the variation of the distributions of colours as a function of spectroscopic and photometric densities. This comparison can only be performed at low redshifts in the SDSS-DR6. Figure 3 shows the colour distributions for the SDSS-DR6, for different luminosity and density bins (different subpanels, see the figure key). Solid lines show the distributions obtained using spectroscopic projected densities; small errorbars computed using Poisson statistics, describe the distributions measured using photometric densities. We have also computed an equivalent colour distribution for the mock catalogues finding that spectroscopic and photometric density estimates are almost indistinguishable. The slight differences in the SDSS-DR6 do not affect the fraction of red galaxies inferred from these diagrams, as it will be shown later in this section. This confirms that photometrically derived densities can be suitable to study the dependence of galaxy colours on environment.

The galaxy population in the low redshift SDSS-DR6 data shows the previously reported behaviour (Balogh et al. 2004; Baldry et al. 2004), where low luminosity galaxies show a transition from a blue, unimodal color distribution to a slightly bimodal distribution including a population of red galaxies as the local density increases. Intermediate luminosities show a clear transition from a blue dominated population to a mostly red population, and high luminosity galaxies show an increasing deficit of blue galaxies. The mock catalogue, on the other hand, shows narrower colour distributions with qualitatively similar behaviours to the observed data. As it has been reported in previous works (cf. Weinmann et al., 2006), the colours in semi-analytic models still fail to reproduce observed values with high accuracy. We do not show colours for low luminosity semi-analytic galaxies due to the completeness limit of the simulation.

As the redshift increases, we find that SDSS-DR6 galaxies show different behaviours depending on their luminosity. The left panel of Figure 4 shows, with different line types, the colour distributions corresponding to different redshift subsamples up to a maximum median redshift of $z = 0.19$; local densities in this figure are obtained using photometric information only. As can be seen, for the high luminosity galaxies (L5), there is no statistically significant trend with local density, regardless of the redshift of the sample; there is a clear trend towards bluer L5 galaxies at higher redshifts, where the red galaxy fraction drops by a $(60 \pm 0.05)\%$ between median $z = 0.052$ and median $z = 0.55$. Fainter galaxies (L2) show a more noticeable shift towards bluer colours, which at low redshifts show the transition from a blue-dominated population to a main population of red galaxies, a $(38 \pm 0.07)\%$ effect.

This seems to be the case also for more intermediate luminosities (L3), which show a similar trend with local density (a $(30 \pm 10)\%$ effect), which becomes clearer at higher redshifts (a $(50 \pm 10)\%$ increase in the red fraction for higher local densities). These results are compatible with those presented by Cucciati et al. (2006), De Lucia et al., (2007) and Ienna & Pelló (2006), who also find a rapid migration to bluer colours as the redshift increases.

The right panel of Figure 4 also shows in different line types the colour distributions for two different redshifts, $0.04 < z < 0.12$ and $0.45 < z < 0.55$ obtained from the evolving mock catalogue using spectroscopically defined densities (errorbars were obtained using photometric density estimates). The main purpose of this panel is to show that colour distributions of galaxies selected according to their photometric estimates of local density, are compatible with those obtained using spectroscopic densities, even at high redshifts. On the other hand, it is noticeable that the evolution of colours in the mock catalogue is qualitatively similar to that in the SDSS in the sense that low luminosity galaxies at high redshifts show a lack of a red galaxy population. The most luminous galaxies in the model become much bluer than observed in the SDSS-DR6. We now turn to make quantitative estimates of the changing colours of the general galaxy population.

A more direct way to characterise the distribution of galaxy colours is via estimates of the red galaxy fraction. This is defined as the ratio between the number of galaxies redder than $u-r = 2.2$ and the total number of galaxies. Figure 5 shows the dependence of this fraction on local density for different galaxy luminosities (increasing luminosity from bottom to top subpanels) and different redshifts (different line types, redshift ranges indicated in the key), for the SDSS data and the no-evolution mock catalogue (left and right panels, respectively). In all subpanels, we show two redshift ranges and spectroscopically and photometrically derived densities. Notice that in the SDSS-DR6 case, we only have spectroscopic data for the low redshift range. As can be seen, the results of the no-evolution mock using either spectroscopic or photometric density estimates show a very good agreement with the underlying lack of evolution, indicating that there are virtually no differences in the red fractions using these two density estimators. In the case of the SDSS-DR6, there is a significant drop in the red galaxy fraction as the redshift increases. For the highest luminosity galaxies (labeled L5), the fraction plummets from a value of $\simeq 0.9 - 1$ to $\simeq 0.3$, remaining constant as the local density increases. Intermediate luminosities (labeled L3), show that the red fraction drops by a 50% between median redshifts of $z = 0.062$ and $z = 0.19$, for low surface densities, $\Sigma/h^2\text{Mpc}^{-2} < 1$; higher densities show a less significant change with redshift.

6 CONCLUSIONS

We have studied the evolution of the distribution of galaxy colours in the SDSS-DR6 at intermediate redshifts $0.04 < z < 0.63$, and its dependence on projected local density, as inferred from nearby neighbours in projection, using photometric redshift information.

A first step consisted in constructing mock catalogues with photometric redshifts and uncertainties derived from the differences between z_{phot} and z_{spec} in the SDSS-DR6 MGS, in two versions, one with an evolving galaxy population and another one with no evolution. These mocks are used for two main purposes, i) to determine whether the statistical analyses are affected by systematic errors, and to assess stochastic errors to improve the determination of projected densities for the analysis on real data, and ii) to com-

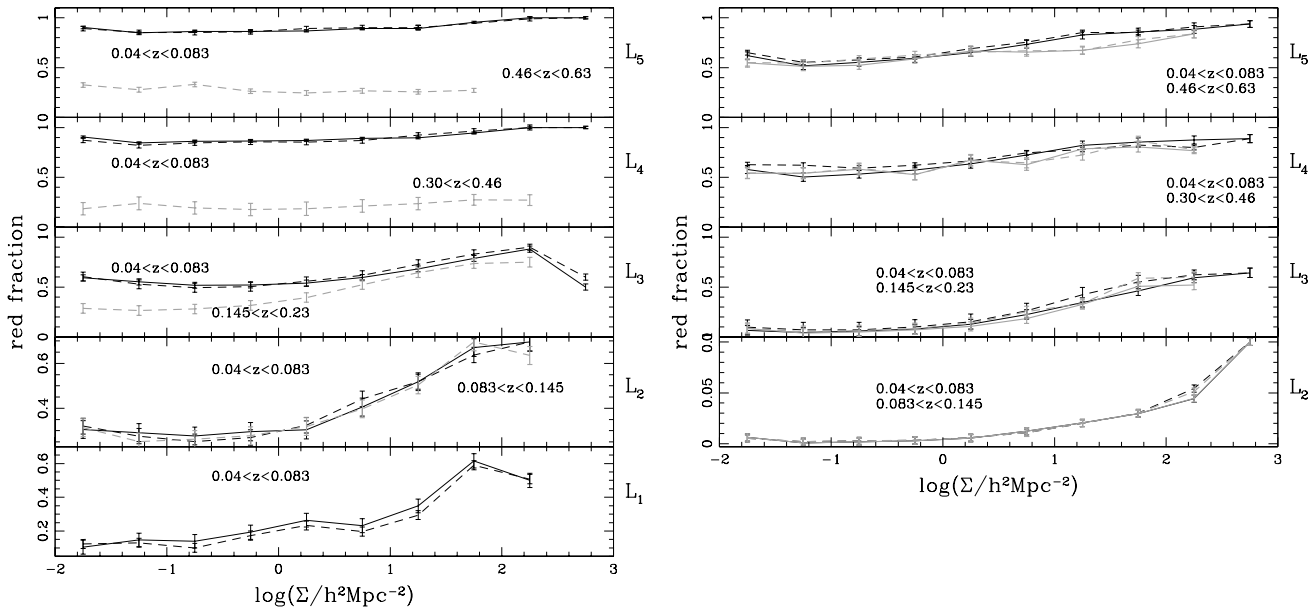


Figure 5. Red galaxy fractions in the SDSS-DR6 and mock catalogues (left and right panels, respectively) for different luminosities (increasing from bottom to top sub-panels), as a function of projected density, Σ , and in different redshift bins (see the figure key). Dashed lines correspond to the red galaxy fraction on the photometric sample for high and low redshift (grey and black lines respectively) and solid lines correspond to the results from the spectroscopic sample.

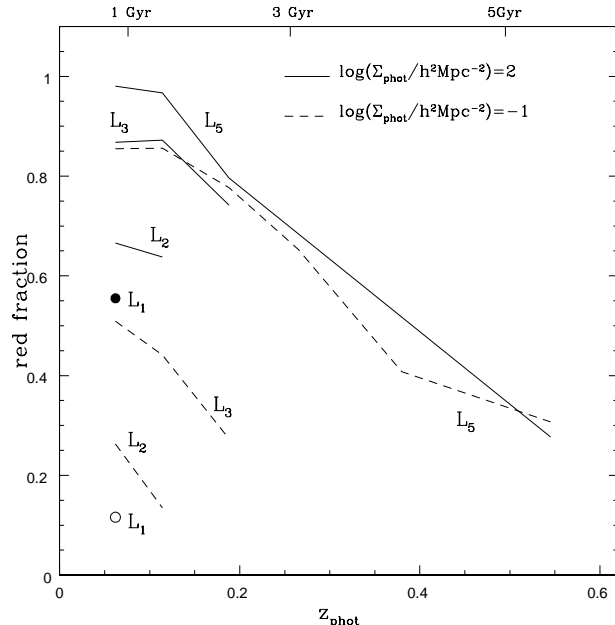


Figure 6. Evolution of the red galaxy fraction in the SDSS-DR6, for two different projected densities (see the figure key).

pare the evolution predicted by the galaxy formation model to the observed evolution.

Using the SDSS-DR6 MGS, we are able to tune our density measurement technique as well as to determine that the estimates of projected densities using photometric redshift information are in agreement with the results using spectroscopic data, out to $z \simeq 0.3$. We confirm this result in the mock catalogues (both with and with-

out evolution), and extend this test out to much higher redshifts, $z = 0.63$, the maximum redshift out to which we can analyse the SDSS-DR6 photometric catalogue avoiding possible confusion problems between galaxies and the PSF. We also test whether the colour distributions of galaxies selected in bins of projected density are comparable when using photometric and spectroscopic distances to select close neighbours for the determination of projected densities. We find that the distributions are compatible both in the real and mock data. In this case, the variations in the colour distributions seen in the model are narrower than in the real data, but follow qualitatively similar trends with density and luminosity. Low luminosity galaxies show mostly a blue population, with signatures of a red population appearing only at the highest density bin; high luminosity galaxies show mostly a red population, with some blue galaxies only at low densities. Intermediate luminosities show a nice transition from a bimodal colour distribution at low densities to an almost unimodal red distribution at high densities. These results are in excellent agreement with previous studies (e.g. Balogh et al., 2004).

The evolution of the colour distributions with redshift shows that low luminosity galaxies tend to loose the red population almost completely, while the blue population shifts to even bluer colours; high luminosity galaxies, on the other hand, show a constant shift to bluer colours; this is more easily seen in our study of red galaxy fractions for different redshift intervals. One important characteristic of this evolution is that the dependence of the red fraction on local density in high luminosity galaxies, $M_r - 5 \log(h_{70}) < -20.5$, retains its overall shape and only changes by a constant shift, which for $-23 < M_r - 5 \log(h_{70}) < -21.5$, corresponds to a $\simeq 60\%$ increase from median $z = 0.545$ to $z = 0.05$. Intermediate luminosities, $-21 < M_r - 5 \log(h_{70}) < -19.5$, show a 50% increase from a median $z = 0.19$ to median $z = 0.05$ in the red fraction in relatively low projected densities; galaxies in high density environments show a milder change in the red fraction in this red-

shift range. This evolution can be more easily seen as a function of redshift for fixed values of local density, as is shown in Figure 6, where solid lines and filled symbols correspond to high densities, and dashed lines and open symbols to very low local densities. As can be seen, the slope in the red fraction evolution is approximately constant implying that in the local universe, the blue fraction decreases at a rate of 15%/Gyr. There is an indication that faint and bright galaxies follow a similar trend, but due to the magnitude limit of the SDSS-DR6, the data on the evolution of the fainter subsamples reaches lower redshifts, increasing the uncertainty in the estimate of the slope.

These results are consistent with previous works (Cucciati et al., 2006, De Lucia et al., 2007, Martínez et al. 2006, Ienna & Pelló, 2006), where the population of high luminosity galaxies becomes red at higher redshifts than their low luminosity counterparts. This phenomenon has been termed “downsizing” in the literature (e.g. Marconi et al. 2004, Shankar et al. 2004), in relation to the star formation activity shifting from larger objects towards smaller galaxies, in apparent contradiction to the hierarchical model of galaxy formation. Several recent works have shown that this behaviour is in fact also natural in a hierarchical Universe (Lagos, Cora & Padilla, 2008, Bower et al., 2006, Croton et al., 2006); however, it still remains a challenge for galaxy formation models to reproduce the actual distribution and evolution of galaxy colours which at present is achieved only qualitatively at best, for which this work provides the most accurate measurements carried out to date.

7 ACKNOWLEDGMENTS

We thank referee for very helpful comments. NP was supported by Fondecyt grant No. 1071006. The authors benefited from a visit of DGL to Santiago de Chile supported by Fondecyt grant No. 7070045. This work was supported in part by the Centro de Astrofísica FONDAF, Consejo Nacional de Investigaciones Científicas y Técnicas de la República Argentina (CONICET), Secretaría de Ciencia y Tecnología de la Universidad de Córdoba. Funding for the SDSS and SDSS-II has been provided by the Alfred P. Sloan Foundation, the Participating Institutions, the National Science Foundation, the U.S. Department of Energy, the National Aeronautics and Space Administration, the Japanese Monbukagakusho, the Max Planck Society, and the Higher Education Funding Council for England. The SDSS Web Site is <http://www.sdss.org/>. The SDSS is managed by the Astrophysical Research Consortium for the Participating Institutions. The Participating Institutions are the American Museum of Natural History, Astrophysical Institute Potsdam, University of Basel, University of Cambridge, Case Western Reserve University, University of Chicago, Drexel University, Fermilab, the Institute for Advanced Study, the Japan Participation Group, Johns Hopkins University, the Joint Institute for Nuclear Astrophysics, the Kavli Institute for Particle Astrophysics and Cosmology, the Korean Scientist Group, the Chinese Academy of Sciences (LAMOST), Los Alamos National Laboratory, the Max-Planck-Institute for Astronomy (MPIA), the Max-Planck-Institute for Astrophysics (MPA), New Mexico State University, Ohio State University, University of Pittsburgh, University of Portsmouth, Princeton University, the United States Naval Observatory, and the University of Washington.

REFERENCES

- Adelman-McCarthy J. K., et al. (The SDSS Collaboration) 2005, *ApJS*, in press (astro-ph/0507711).
- Baldry, I. K., Balogh, M. L., Bower, R., Glazebrook, K., & Nichol, R. C. 2004, *AIP Conf. Proc.* 743: *The New Cosmology: Conference on Strings and Cosmology*, 743, 106
- Balogh, M., et al. 2004, *MNRAS*, 348, 1355
- Benítez, N. 1998, Abstracts of the 19th Texas Symposium on Relativistic Astrophysics and Cosmology, held in Paris, France, Dec. 14-18, 1998. Eds.: J. Paul, T. Montmerle, and E. Aubourg (CEA Saclay), meeting abstract.,
- Benítez, N. 2000, *ApJ*, 536, 571
- Blanton, M. R., et al. 2003, *AJ*, 125, 2348
- Blanton, M., & Roweis, S. 2007, *AJ*, 133, 734.
- Bolzonella, M., Miralles, J.-M., & Pelló, R. 2000, *A&A*, 363, 476
- Bower, R. G.; Benson, A. J.; Malbon, R.; Helly, J. C.; Frenk, C. S.; Baugh, C. M.; Cole, S.; Lacey, C. G., 2006, *MNRAS*, 370, 645.
- Brunner, R. J., Djorgovski, S. G., Gal, R. R., & Odewahn, S. C. 1999, *Bulletin of the American Astronomical Society*, 31, 1492
- Bruzual, G. & Charlot, 2003. Djorgovski, S. G., Gal, R. R., & Odewahn, S. C. 1999, *Bulletin of the American Astronomical Society*, 31, 1492
- Collister, A. A., & Lahav, O. 2004, *PASP*, 116, 345
- Coldwell & Lambas G. 2006, submitted
- Connolly, A. J., Csabai, I., Szalay, A. S., Koo, D. C., Kron, R. G., & Munn, J. A. 1995, *AJ*, 110, 2655
- Croton, D., et al., 2006, *MNRAS*, 365, 11.
- Csabai, I., et al. 2003, *AJ*, 125, 580
- Cucciati, O., et al. (The VIMOS VLT Deep Survey Team) 2006, *A&A*, 458, 39.
- De Lucia, G., et al. 2007, *MNRAS*, 374, 809.
- Dressler, A. 1980, *ApJ*, 236, 351
- Eisenstein, D. J., et al. 2001, *AJ*, 122, 2267
- Fukugita, M., Ichikawa, T., Gunn, J. E., Doi, M., Shimasaku, K., & Schneider, D. P. 1996, *AJ*, 111, 1748
- Gómez, P. L., et al. 2003, *ApJ*, 584, 210
- Gonzalez, A.H., Zaritsky D., Dalcanton, J.J., Nelson, A., 2001, *ApJS*, 137, 117.
- Gunn, J. E., et al. 1998, *AJ*, 116, 3040
- Gwyn, S. D. J., & Hartwick, F. D. A. 1996, *ApJL*, 468, L77
- Hogg, D. W., Blanton, M.,
- Ienna, F., & Pelló, R. 2006, *SF2A-2006: Semaine de l’Astrophysique Française*, 347 & *SDSS Collaboration 2001, Bulletin of the American Astronomical Society*, 34, 570
- Koo, D. C. 1985, *AJ*, 90, 418
- Lagos, C., Cora, S., & Padilla, N. 2008, *MNRAS*, submitted.
- Marconi A., Risaliti G., Gilli R., Hunt L., Maiolino R., Salvati M., 2004, *MNRAS*, 351, 169
- Martínez, H. J., O’Mill, A. L., & Lambas, D. G. 2006, *MNRAS*, 372, 253
- Oyaizu, H., Lima, M., Cunha, C. E., Lin, H., Frieman, J., & Sheldon, E. S. 2008, *ApJ*, 674, 768
- Pier, J. R., Munn, J. A., Hindsley, R. B., Hennessy, G. S., Kent, S. M., Lupton, R. H., & Ivezić, Ž. 2003, *AJ*, 125, 1559
- Richards, G. T., Hall, P. B., Vanden Berk, D. E., Schneider, D. P., Strauss, M. A., & Fan, X. 2002, *Bulletin of the American Astronomical Society*, 34, 1309
- Schneider, D. P., et al. 2003, *AJ*, 126, 2579
- Scranton, R., et al. 2002, *ApJ*, 579, 48.
- Shankar F., Salucci P., Granato G., De Zotti G., Danese L., 2004,

- MNRAS, 354, 1020
- Smith, J. A., Tucker, D. L., Allam, S. S., & Jorgensen, A. M. 2002, Bulletin of the American Astronomical Society, 34, 1272
- Springel V., White S. D. M., Jenkins A., Frenk C. S., Yoshida N., Gao L., Navarro J., Thacker R., Croton D., Helly J., Peacock J. A., Cole S., Thomas P., Couchman H., Evrard A., Colberg J., Pearce F., 2005, Nature, 435, 629
- Strauss, M. A., et al. 2002, AJ, 124, 1810
- Stoughton, C., et al. 2002, AJ, 123, 485.
- Weinmann, Simone M.; van den Bosch, Frank C.; Yang X.; Mo, H.J.; Croton, D.J. et al, 2006, MNRAS 372, 1161
- York, D. G., et al. 2000, AJ, 120, 1579